ELSEVIER

Journal of Structural Geology 27 (2005) 1300–1314

JOURNAL OF STRUCTURAL GEOLOGY

www.elsevier.com/locate/jsg

A 3D study of aligned porphyroblast inclusion trails across shear zones and folds

P.M. Evins*

Department of Geology, University of Oulu, Linnanmaa, 90570 Oulu, Finland

Received in revised form 27 January 2004
Available online 16 February 2005

Abstract

Inclusion trails (S_i) within 741 equant garnet porphyroblasts show a consistent orientation across a 100 m^2 outcrop of Precambrian metapelite with later (D_2) folds and shear zones in Posio, Finland. Variation in S_i orientations is not systematic with respect to these later folds and shear zones, but instead represents microfolding and warping of S_1 before the formation of D_2 structures. The development of the D_2 folds and shear zones is investigated by comparing the pattern of S_i in the outcrop to those predicted for porphyroblasts in tangential longitudinal strain, axial slip, flexural flow, pure shear, partitioned flexural flow and partitioned pure shear folds. S_i patterns are also compared with models for non-coaxial and coaxial shear zones. Along with corroborating evidence from structures in the outcrop and matrix, the comparisons indicate that D_2 folds and shear zones in the outcrop formed in response to NW–SE axially symmetric shortening during which garnet porphyroblasts did not rotate relative to each other, the axial plane of F_2 folds, and D_2 shear zone boundaries.

Keywords: Inclusion trails; Microfolds; Shear zones; Fold mechanisms; Rotation

1. Introduction

For over a decade, the debate has continued between those who argue that porphyroblasts do not rotate with respect to the geographic reference frame or other external reference frames, such as fold axial planes and external foliation, and those who suggest they do rotate relative to some external reference frame during deformation (e.g. Bell, 1985; Bell et al., 1992; Passchier et al., 1992; Johnson, 1993, 1999; Kraus and Williams, 2001). Aside from this general debate, porphyroblast microstructures have been shown to reveal a wide array of valuable geological information in studies ranging from P–T–D–t paths to magma emplacement to shear-strain rates. A relatively recent application has been the use of porphyroblast-matrix–fold relationships to evaluate fold mechanisms (Williams and Jiang, 1999; Jiang, 2001; Stallard and Hickey, 2001). Williams and Jiang (1999) and Jiang (2001) devised a method for assessing fold mechanisms and some rheological information based on equations for the rotational behaviour of rigid spherical particles (i.e. porphyroblasts) from 2D fluid mechanics (e.g. Jeffery, 1922). Their theoretical predictions have been successfully reproduced by Stallard and Hickey (2001) with a large 3D dataset of snowball garnets from a polyphase deformed schist. Consistent patterns of straight inclusion trails (S_i) across macro- to mesoscopic folds have been used as arguments in favour of both rotational and non-rotational porphyroblast behaviour (e.g. Fyson, 1980; Steinhardt, 1989; Johnson, 1990a,b; Visser and Mancktelow, 1992; Forde and Bell, 1993; Aerden, 1995; Kraus and Williams, 1998; Ilg and Karlstrom, 2000). Many of these studies are limited by a paucity of data, lack of 3D data and reliance on regional correlations (Passchier et al., 1992). This contribution presents a large database of the 3D orientation of garnet porphyroblast inclusion trails from an outcrop of mica schist with later folds and shear zones. The method of Williams and Jiang (1999) was applied to this dataset to better understand the development of the folds. The outcrop is located in the central part of the Posio shear zone in the village of Posio in eastern Finland (Fig. 1).

* Corresponding author. Current address: Economic Geology Research Unit, School of Earth Sciences, James Cook University, Townsville, 4811 QLD, Australia.
E-mail address: paul.evins@jcu.edu.au.

0191-8141/$ - see front matter © 2004 Elsevier Ltd. All rights reserved.
doi:10.1016/j.jsg.2004.08.003

2. Regional setting of the Posio outcrop

The N–S-trending, steeply W-dipping Hirvaskoski shear zone (HSZ) splits the Archaean craton of north-central Finland into the Kuhmo block to the east and the Pudasjärvi block to the west (Fig. 1). It is a dextral shear zone that is part of the 1860–1850 Ma (Vaasjoki et al., 2001) D_2 Savolappi shear system characterised by left stepping, N–S-trending, steep ductile shear zones (Kärki et al., 1993). The northern tip of the HSZ bifurcates as it enters the granitoids and gneisses of the Central Lapland Granitoid complex and its NE-trending central arm has been labelled the Posio

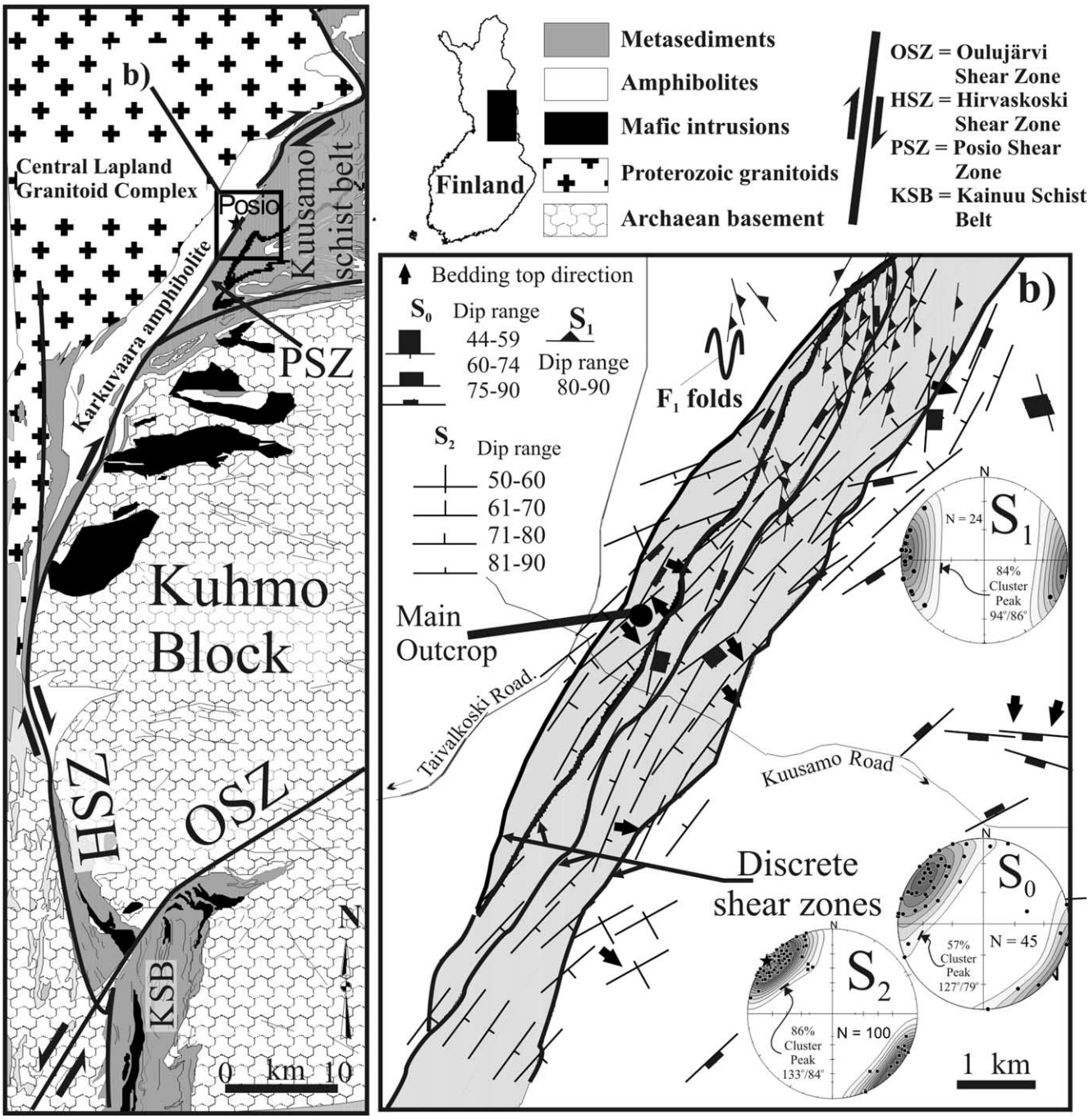

Fig. 1. (a) The Posio shear zone and surrounding tectonic elements. (b) The Posio region containing the Posio shear zone (grey) between the Karkuvaara metalavas and Kuusamo supracrustal belt. Opposite top directions within the shear zone suggest that S_0 has been isoclinally folded and transposed parallel to S_2. Equal-area projections in the bottom right reflect the subparallelism of S_0, S_2 and the general trend of the Posio shear zone (star). Outside of the shear zone, the distribution and orientations of S_0 and top directions define broader, complex folds in the Kuusamo belt. N–S-trending F_1 folds and S_1 foliations (plotted in the equal-area projection to the upper right) are only visible in the northern half of the area. Further south, they have been destroyed, transposed or completely overprinted by D_2. The map displays spatially averaged planar fabric orientations.

shear zone (PSZ). The PSZ cuts the western margin of the early Proterozoic Kuusamo schist belt bounded to the west by the Karkuvaara amphibolite-facies metalavas and to the east by the Kirintövaara quartzite of the Kuusamo belt. Further north, it separates the Archaean–Proterozoic metaplutonic Central Lapland Granitoid complex from the Kuusamo belt. The PSZ follows a 2-km-wide belt of muscovite–biotite ± garnet ± staurolite ± kyanite metapelites and turbiditic metapsammites. Similar lithologies are found further south within the Kainuu schist belt deformed by the HSZ (Tuisku and Laajoki, 1990). Isoclinal F_1 folds with N–S-trending, subvertical axial planes are found in the more competent Karkuvaara amphibolites, and an axial planar S_1 is found in more resistant shear pods of the PSZ to the north of the examined outcrop. Most of these earlier D_1 structures in the PSZ have been either transposed into or destroyed by the D_2 shear zones that characterise the PSZ (Fig. 1b). As a continuation of the HSZ, the PSZ shows evidence of dextral shear in the form of Z folds and crenulations north and south of the Posio outcrop. However, several NE-trending structures north of the PSZ have been attributed to regional NW–SE shortening perpendicular to their strike (Evins and Laajoki, 2002; Evins et al., 2002).

3. The Posio outcrop

3.1. Main features

The Posio outcrop is a 12 × 3 m pavement exposure of thinly bedded (≤20 cm) sandy turbidites (domain I) and laminated garnet–staurolite–muscovite–biotite schist (Figs. 2 and 3). The schist can be divided into lower strain areas of folded compositional layering where bedding is still recognisable (Fig. 3, domains III, V, and VII) and higher strain zones where the fold limbs have been attenuated, compositional layering has been transposed, and bedding is unrecognisable (Fig. 3, domains II, IV, and VI).

3.2. Compositional layering

Bedding is defined by 1-mm-wide biotite lamellae at the top of individual 2–5-cm-wide pelite beds. In thin section, the lamellae are composed almost entirely of biotite oriented parallel to S_2. Occasionally, in the thicker layers, graded bedding can be identified as a decrease in quartz and feldspar grain size accompanied by a gradual increase in Fe- and Al-rich minerals towards the top of each bed. Most individual beds cannot be followed more than a metre along strike on the outcrop; so compositional layering may not represent a simple succession of sedimentary layers. In the higher strain domains, layer thickness decreases to 1 cm or less and the origin of biotite lamellae comes into question (Fig. 4). Compositional layering in the schists is more likely a composite S_0/S_1 layering resulting from early F_1 isoclinal folding of S_0, although no F_1 fold noses were observed at the

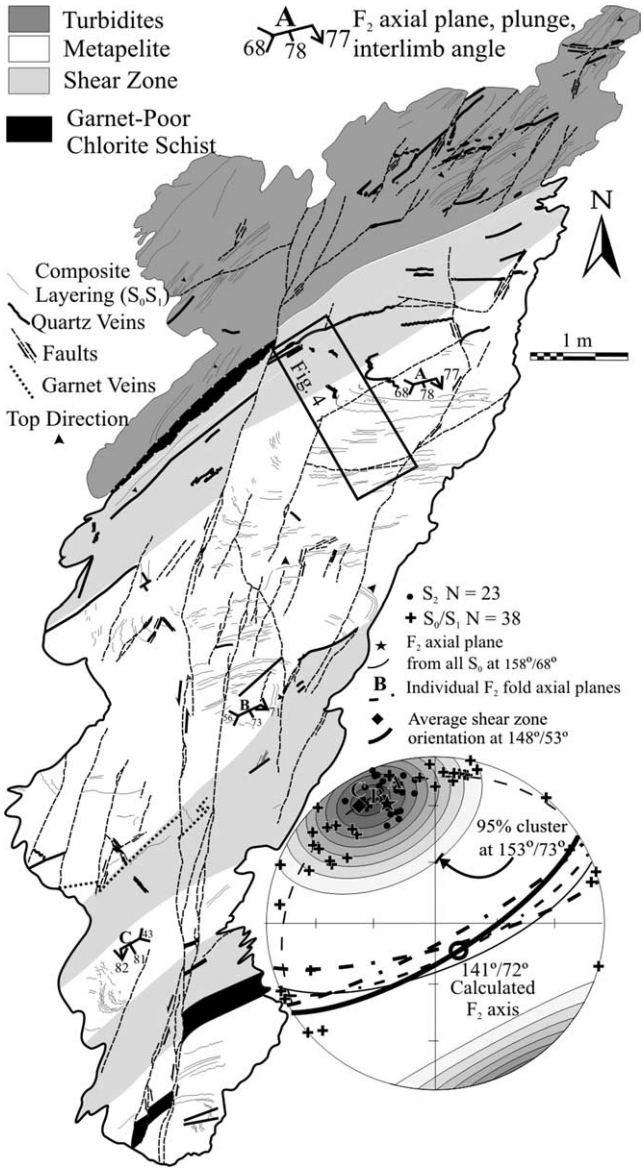

Fig. 2. Features of the Posio outcrop include folded composite S_0/S_1 compositional layering and quartz veins and a network of later, dominantly sinistral, brittle faults. The equal-area projection of poles to planar fabric elements demonstrates the parallelism between S_2 (contoured), individual F_2 fold axial planes, and the mean orientation of D_2 shear zones in the main outcrop. The F_2 fold axis is calculated from the girdle defined by S_0/S_1 compositional layering and is similar in orientation to individual F_2 fold axes.

outcrop. However, isoclinal F_1 folds have been identified 1 km north of the area (Fig. 1) and opposing top directions in turbidite beds from adjacent outcrops indicate that the sediments have been isoclinally folded before the formation of D_2 structures. The absence of a reliable, continuous S_0 represents an important limitation for investigating later folding mechanisms.

3.3. Garnet porphyroblasts

Due to its lower resistance to weathering, the schist

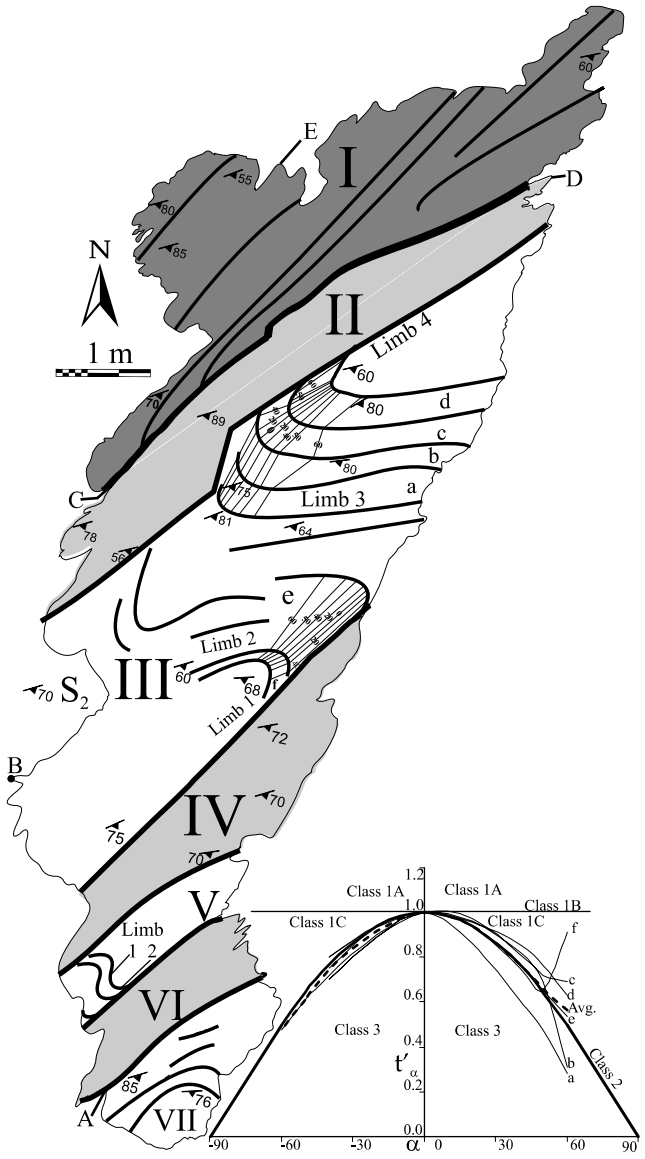

Fig. 3. Generalised sketch of F_2 folds and shear zones with axial planar S_2 foliation measurements. Apparent dip isogons are shown for the two major folds in domain III. Removal of the displacement of the later faults and rotation of the folds into the fold profile plane does not change the pattern significantly but was necessary for applying Ramsay's (1967, pp. 360–370) tangential thickness method shown bottom right. t'_α is layer thickness/layer thickness at the fold hinge and α is the dip of the layer in degrees. Both dip isogon and tangential thickness analyses indicate that the folded layers alternate from Class 1C to Class 3 geometries, approximating an overall Class 2 similar fold geometry. Reference coordinates A–E can be found in the outcrop database in the online version of this article at doi:10.1016/j.jsg.2004.08.003.

matrix was preferentially weathered leaving garnets exposed 5–10 mm above the matrix This allowed the measurement of the 3D orientation of S_i within garnet. Garnet porphyroblasts vary from 1 to 2 cm in diameter and are usually equant. Some parts of the outcrop contain oblate garnets with axial ratios up to 2:2:1. These oblate garnets are consistently dimensionally oriented parallel to their well developed internal S_i (Fig. 5e) suggesting that they grew parallel to compositional layering. Most of the garnets are spherical, however, and many have 1-mm-wide, euhedral, inclusion-free rim overgrowths. The angular shape of these garnets is important when comparing their behaviour with that of ideal spheres or ellipsoids during analysis of folding mechanisms. EDS (energy dispersive X-ray spectroscopy) profiles from equant garnets on different fold limbs and oblate garnets in shear zones show a smooth decrease in weight percent MnO and CaO and increase in FeO and MgO from core to rim with steepening of slopes where inclusion free rims begin (Fig. 5f). Similarity between garnet size, morphology and compositional profiles in different fold limbs and shear zones indicates they all grew at the same time (Fig. 5). In the SW part of the outcrop, prominent 3-cm-wide veins composed of coarse (1 cm) subhedral garnet, quartz, and sericitised feldspar mark the boundary between domains IV and V. Incidentally, garnets in these veins share similar compositions to the other garnets in the outcrop. Garnets in the Kainuu schist belt further south have grown before or during regional dextral D_2 deformation (Laajoki and Tuisku, 1990).

3.3.1. Garnet strain shadows

The detailed geometry of garnet inclusion trails and strain shadows was deduced from orthogonal thin sections of several samples from the outcrop and is schematically represented in Fig. 5a. Strain shadows are composed solely of coarser, undulatory, recrystallised, elongate quartz grains and occasional muscovite that define a fabric that is usually continuous with garnet S_i (Fig. 5). In the surrounding matrix, quartz appears much more deformed (sutured and fine-grained recrystallised grain boundaries) and muscovite and biotite are several times more abundant. The strain shadows extend up to 1 cm from garnet porphyroblasts and indicate that D_2 deformation outlasted garnet growth. Their 3D shape is generally symmetrical, oblate (slightly longer vertically) and parallel to the dominant S_2 foliation that surrounds them, *irrespective of location* in the outcrop (Figs. 4 and 5). Strain shadows also completely fill the gaps between garnets within 1 cm of each other and preserve garnet inclusion trails across the gaps (Fig. 5c and d).

3.3.2. Garnet inclusion trails (S_i)

Garnet S_i is defined by preferentially oriented, elongate, slightly undulatory, recrystallised quartz inclusions and occasionally by opaque minerals (Fig. 5). Some garnets display rhythmic inclusion-free/inclusion-rich layering of variable width that may be inherited from compositional differentiation. In most thin sections, S_i is truncated by a 1 mm rim of inclusion free garnet at the strain caps and is continuous with the external foliation (S_e) in the strain shadows. Roughly two-thirds of unrimmed garnets display continuity between S_i and S_e in the matrix. Inclusion trail geometries were constrained from individual sets of three orthogonal thin sections (one parallel to S_2 and two mutually perpendicular to S_2) plus one oblique thin section. In horizontal and vertical thin sections perpendicular to the

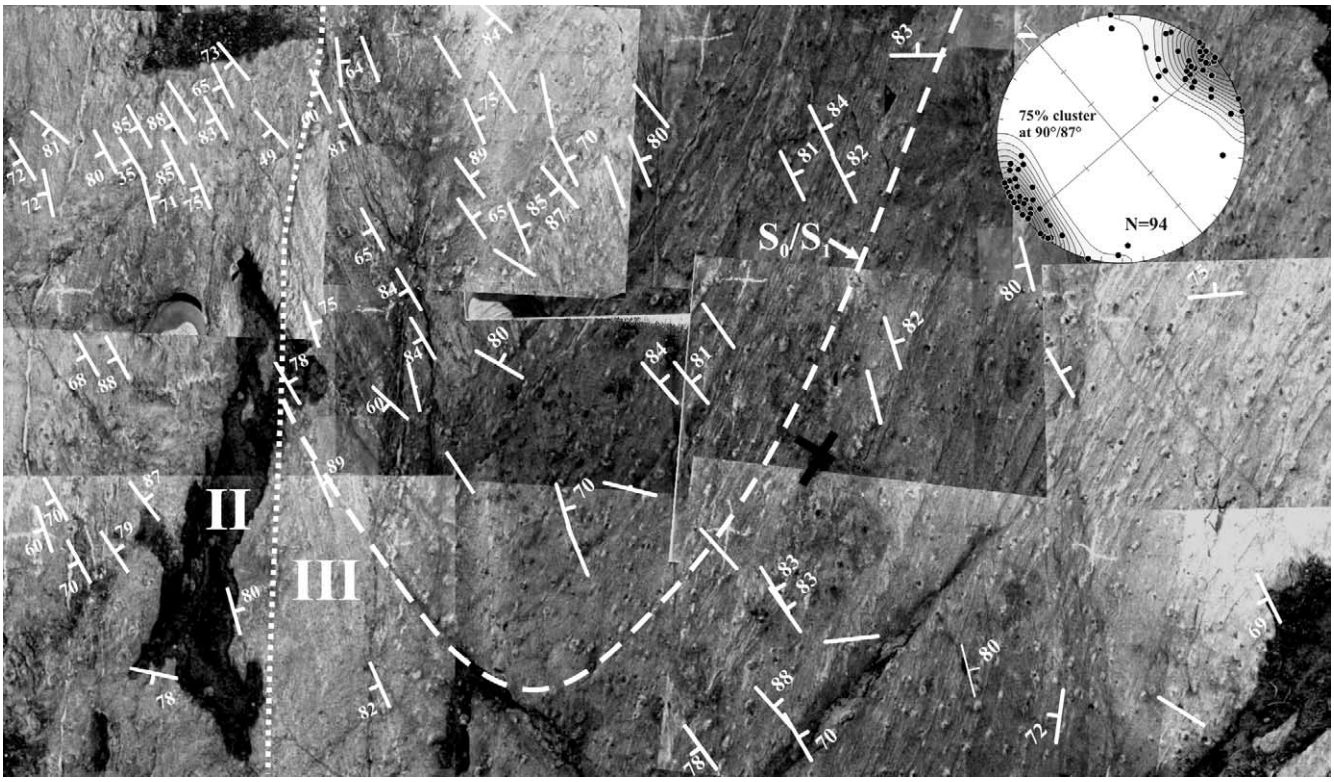

Fig. 4. Photomosaic from the section of outcrop delineated in Fig. 2 with raw garnet S_i plotted over measurement locations and on the equal-area projection. Inspection of the geometry of garnet strain shadows on this horizontal surface yields symmetric strain shadows for 81 and 90% of the garnets in the shear zone domain (II) and fold domain (III), respectively. Of the 395 garnet strain shadows observed from this mosaic, 90% are symmetric.

dominant D_2 schistosity, garnet inclusion trails are straight (Fig. 5b and c). Less than 5% of the trails in these sections are curved. However, thin sections parallel to the dominant S_2 schistosity reveal open (120° interlimb angle), centimetre-wavelength, Class 1C microfolds of S_i along subhorizontal axial planes with NW–SE plunging subhorizontal axes in both garnets and their strain shadows (Fig. 5d). This type of S_i curvature is found only in thin sections approaching parallelism with the external foliation (S_2) and is usually asymmetric and found near garnet rims. However, these internal foliation deflections occasionally occur as a symmetric fold closer to garnet cores. Where they are curved, individual inclusion trails tend to remain parallel or diverge slightly approaching garnet rims. Areas of curvature near the rims show a less pronounced steepening of EDS profiles than inclusion free rims (Fig. 5f). Due to the subhorizontal orientation of the axis and axial plane of these microfolds, they were not detected while measuring the 741 garnet inclusion trails on the horizontal surface.

3.4. D_2 structures

3.4.1. F_2 folds and associated shear zones

Mesoscopic F_2 folds (domains I, III, V, and VII) are separated by ~1 m wide shear zones (domains II, IV, and VI) in which compositional S_0/S_1 layering is transposed parallel to the dominant, NE-trending S_2 schistosity. Approximately 2.5 m wavelength F_2 folds of S_0/S_1 compositional layering plunge steeply SE with steeply dipping, NE-trending axial planes. Their interlimb angles range from 43 to 68°. Centimetre-scale parasitic folds with synthetic asymmetry are occasionally found in discontinuous biotite-rich bedding tops (Fig. 2). Both dip isogon and tangential thickness analyses (Ramsay, 1967, pp. 360–370) from the two folds in domain III indicate that the folded layers alternate from Class 1C to Class 3 geometries approximating an overall Class 2 similar fold geometry (Fig. 3). Where these folds enter the higher strain domains of the outcrop, compositional layering thickness decreases dramatically from 2–5 cm to less than 1 cm (Fig. 4). In essence, these shear zones could be classified as Ramsay and Lisle's (2000, pp. 862–866) F- or P-bands or simply high strain limbs of similar folds. From their limited exposure along strike (Fig. 2), the shear zone boundaries are curvilinear and may anastomose as seen on a larger scale in the PSZ (Fig. 1). The mean orientation of the shear zones is within 10° of the axial plane of F_2 folds (Fig. 2) implying that they formed during the same event. A 15 cm wide, NE (136°/67°)-trending fault along the NW side of domain II separates the turbidites from the schists. A similar choritised zone is found along the SE side of domain VI. Chloritisation and removal of garnet along these zones suggests they may

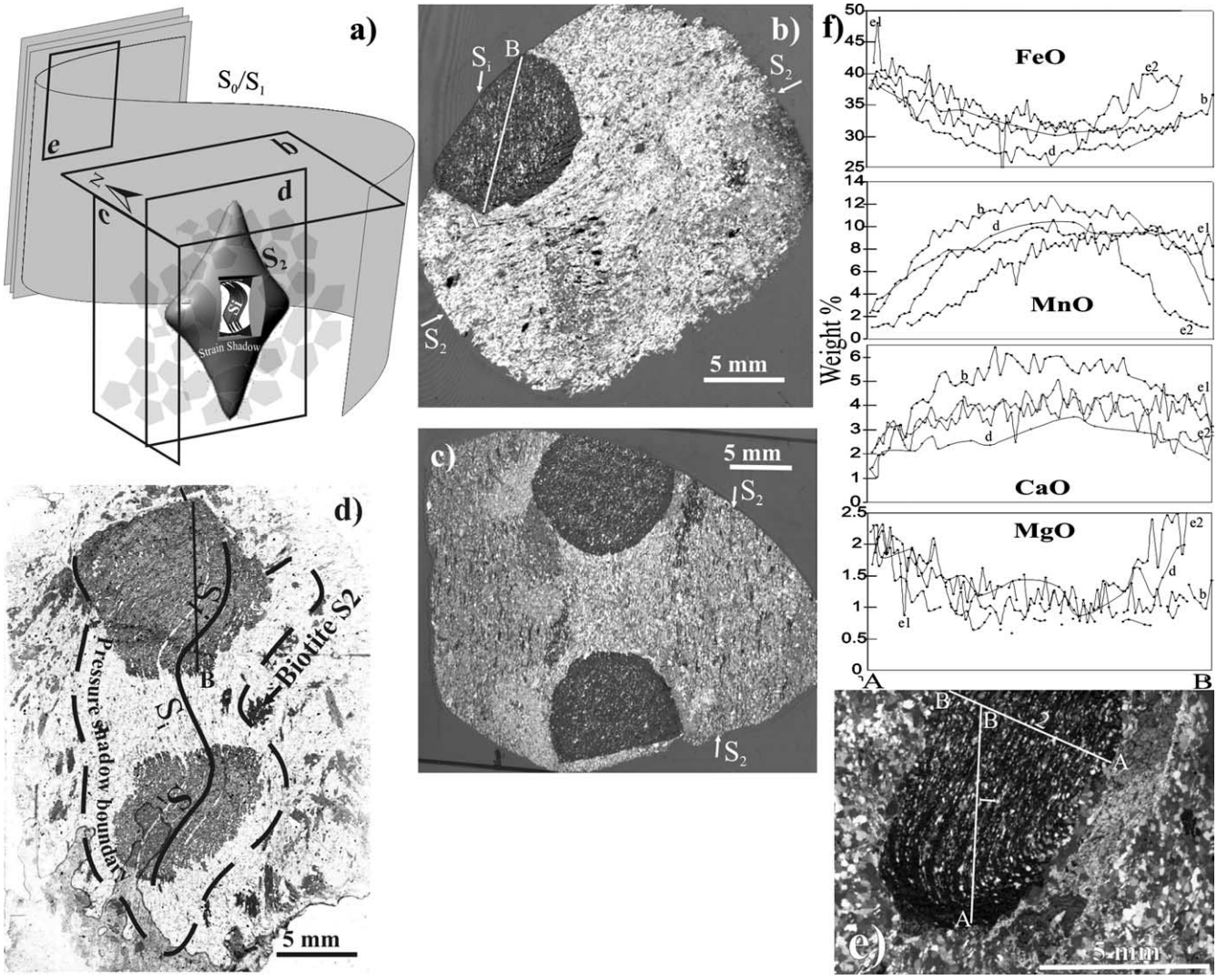

Fig. 5. (a) Schematic diagram of relationships between garnet S_i and the garnet strain shadow, S_2 schistosity, and F_2 folded S_0/S_1 compositional layering. This image is an interpretation of individual sets of four thin sections: three orthogonal thin sections (one vertical thin section parallel to S_2, one vertical thin section perpendicular to S_2 and one horizontal thin section perpendicular to S_2) and one thin section roughly bisecting the two vertical thin sections. Thin sections described below were taken from the labelled planes b–e. (b) Thin section of a horizontal plane oriented perpendicular to S_2 showing straight garnet S_i (oriented N–S) oblique to S_2 (oriented NE–SW). Note the euhedral, inclusion free rim on the bottom of the garnet. Sample is from limb 3 of domain III. Crossed nicols. (c) Thin section of a vertical plane oriented perpendicular to S_2 showing two garnets with poorly developed S_i joined by a strain shadow. S_2 schistosity in the matrix is continuous leaving no evidence of earlier folding or crenulations in the recrystallised quartz regions between the mica domains. Sample is from limb 3 of domain III. Crossed nicols. (d) Thin section of a vertical plane parallel to S_2 schistosity showing open, recumbent microfolds that continue through the pressure shadow that joins two garnets. Sample is from limb 4 of domain III. (e) Thin section of a vertical plane subparallel to S_2 schistosity showing curvature confined to the rim of an elongate garnet from the shear zone in domain II. Note the presence of staurolite (light grey) on the right side of the garnet. Crossed nicols. (f) EDS profiles across garnets from images b, d and e (profiles labelled accordingly). Number of spot analyses for profiles b, d, e1 and e2 were 20, 59, 83, and 65, respectively. Probe conditions for EDS traverses across garnets were: 20 kV accelerating voltage, 10 nA beam current, 15 mm working distance and 40 s live time.

have acted as a conduit for metasomatic fluids allowing for some volume changes in the shear zone domains during or after their formation.

3.4.2. Dominant schistosity (S_2)

The NE-trending dominant schistosity (S_2) is defined by preferentially oriented, large (up to 2 mm) subhedral biotite, smaller (<1 mm) subhedral muscovite, and elongate (< 1 mm) granoblastic quartz with slightly undulatory extinction. Retrograde chlorite replaces biotite and muscovite in the matrix, strain shadows, and small cracks at garnet rims. As stated earlier, the S_2 foliation wraps around garnet porphyroblasts and their strain shadows (Fig. 5). The foliation is penetrative, with extremely straight mica-rich domains separating recrystallised quartz-rich domains devoid of crenulations. This is reflected by the very consistent orientation (95% cluster, see Appendix A) of S_2, which also indicates little or no refraction across layer

boundaries. The foliation only appears to anastomose around garnets and their strain shadows. S_2 schistosity is usually slightly oblique to individual F_2 fold axial planes, but it is within 5° of the overall F_2 axial plane calculated from all bedding measurements and the average orientation of D_2 shear zones (Fig. 3). There is a substantial difference (20°) between the orientation of S_2 in the outcrop (Fig. 3) and S_2 in the Posio region (outlined by Fig. 1b); however, both represent the latest foliation forming stage of deformation. A few biotite grains oriented at high angles to S_2 are kinked in a manner consistent with flattening perpendicular to the dominant S_2 foliation. The only lineation visible in the investigated outcrop is a weak, subvertical intersection lineation between S_0/S_1 and S_2.

3.5. Post-D_2 staurolite porphyroblasts

Large (up to 1.5 cm) subhedral–anhedral, staurolite poikiloblasts are present as pseudomorphs of biotite and muscovite along garnet porphyroblast and strain shadow margins and in various parts of the matrix (Fig. 5b, c and e). Staurolite never occurs in garnet strain shadows. S_2 is preserved within the poikiloblasts, as parallel elongate quartz and opaque inclusions. Deformation ceased shortly after the growth of staurolite, as shown by a slight deflection of S_2 around the edges of rare, large, euhedral porphyroblasts. In some cases, staurolite is completely replaced by a late phase of white mica. Staurolites further south, in the Kainuu Schist belt, grew after D_2 dextral shearing along the HSZ and before D_4 sinistral shearing along the Oulujärvi Shear Zone (Fig. 1) (Tuisku and Laajoki, 1990; Kärki et al., 1993).

3.6. Quartz veins

Several thin (1 cm) quartz veins are found across the outcrop (Fig. 2). Some are affected by F_2 folds; some are boudinaged, and others strike along fault planes. Those oriented subparallel to S_2 schistosity display boudinage or tight, asymmetric Z-folds with boudinaged limbs parallel to S_2 foliation. Quartz veins at high angles to the S_2 foliation display symmetric, buckled fold trains with enveloping surfaces perpendicular to S_2.

3.7. Late faults

Quartz veins and all other structures are sinistrally offset by a major NE (29°)-trending vertical brittle fault system. The brittle fault system achieves considerable displacement (>10 m) distributed along an anastomosing millimetre- to metre-scale network of single fault planes with individual horizontal displacements of up to 1 m (Fig. 2). A less-developed, vertical, NE-trending conjugate dextral fault set complements the system. Based on the similarity of D_2 structural orientations across the faults, the rotational component of displacement along the faults is minimal.

3.8. Structural synthesis of outcrop features

Although regionally the PSZ appears to be a dextral shear zone (Kärki et al., 1993), most observations from the Posio outcrop are indicative of coaxial deformation. The geometry of alternating shear zones and asymmetric folds mimics a macroscopic dextral crenulation cleavage, however, these relationships can also be interpreted as a result of coaxial NW–SE shortening assuming S_0/S_1 compositional layering was originally oriented N–S parallel to S_1 in the Posio region (Fig. 1b). The orientation of buckled quartz veins and biotite grains and veins displaying asymmetric folds and boudinage (Fig. 3) are also consistent with differential response to pure shear by veins of different original orientations (Talbot, 1970). The orthorhombic symmetry of garnet strain shadows (Fig. 5) strongly suggests that they were formed during shortening normal to the S_2 foliation and nearly equal extension in all directions (slightly more in the vertical direction) within the S_2 foliation plane in a manner approaching axially symmetric shortening depicted by Hobbs et al. (1976, p. 27). Any significant component of simple shear would impose a monoclinic or triclinic symmetry on the strain shadows. Coupled with the lack of asymmetry or any lineation in the outcrop, these observations support a minimal component of simple shear during the history of D_2 at the Posio outcrop.

4. Interpretation of garnet S_i

S_i patterns in orthogonal thin sections (two mutually perpendicular and one parallel to S_e) approximate those portrayed by Powell and Treagus (1967, p. 810) with one important difference. The sigmoidal S_i patterns that are usually found in cross-sections perpendicular to external foliation are instead found on the external foliation plane in this study (Fig. 5a). In other words, the axis of S_i curvature is perpendicular to the external foliation (S_2), F_2 fold axes, and D_2 shear zones. Continuity of S_i microfolds through strain shadows, non-convergent S_i at the curved rims and microfold noses near the centre of some garnets indicate that garnet growth likely occurred after the deformation responsible for S_i curvature. On the other hand, the location of S_i curvature and asymmetry at the compositionally distinct edges of most of the porphyroblasts suggests a later stage of garnet growth may have occurred during deformation. The under-representation of shallower S_i dips (Fig. 6) may be a result of this concentration of curvature near garnet edges that may have been eroded away on the measuring surface. In conclusion, these microfolds may be either relict helictic folds or a consequence of garnet rotation between D_1 and D_2, but due to their orientation with respect to D_2 structures, they bear little relevance to the nature of D_2 deformation.

Over the entire outcrop S_i is dominantly oriented N–NE, represented by a 78% cluster with the mean orientation

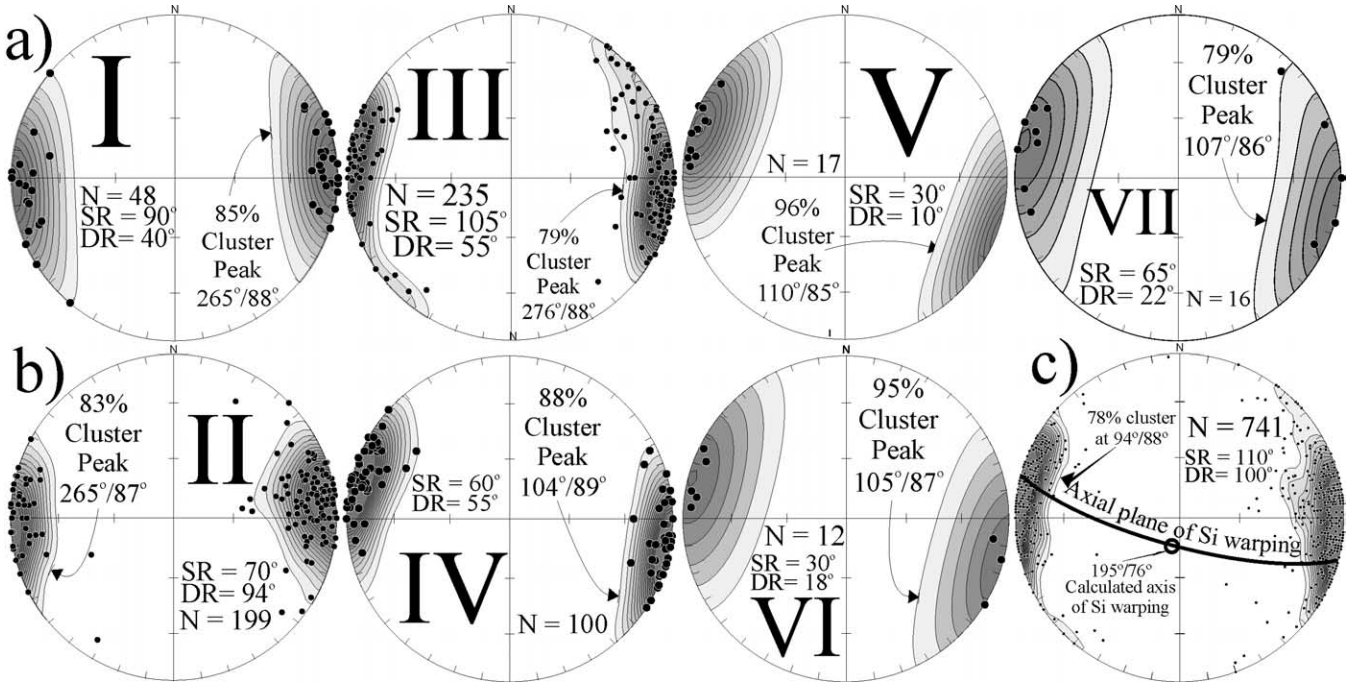

Fig. 6. Lower hemisphere equal-area projections showing the consistency of garnet S_i orientations within (a) F_2 fold domains, (b) D_2 shear zones and (c) the entire outcrop. SR = strike range, DR = dip range. Also plotted in (c) are the calculated axis and axial plane of S_i warping, which are 54 and 36° off from the calculated F_2 fold axis and axial plane, respectively.

striking 12° and dipping vertically (Figs. 6c and 7). Furthermore, the orientations of 103 elongation planes of oblate garnets (Fig. 7) are remarkably consistent (85% cluster) and parallel to equant garnet S_i. Garnet inclusion trails are very similar in orientation (less than a 15° difference in mean orientation) across and within F_2 fold domains III, V and VII (79–96% cluster) and high strain domains IV and VI (88–95% cluster). S_i strike varies more in the high strain domains, while S_i dip varies more in the fold domains (Fig. 6). S_i orientations in domains I and II in the northern part of the outcrop deviate from the average N–NE trend due to a systematic warping of S_i trend lines across the outcrop revealed by spatial averaging of orientation data. Spatial analysis of both equant and oblate garnet S_i on the outcrop scale reveals gentle, 10-m-wavelength, vertically plunging Class 1B folds with E–W-trending axial planes (Fig. 6c) and a 145° interlimb angle (Fig. 7). The angles between the axis and axial plane of this gentle warping and the mean F_2 fold axis and axial plane are 54 and 36°, respectively (Figs. 2 and 6c). These spatial and orientation differences between macroscopic S_i folds and D_2 features in the outcrop indicate that the S_i folds did not form during D_2. The folds are likely pre-D_2 based on the absence of any folds of similar appearance and orientation overprinting or disturbing D_2 structures in the outcrop.

Variations in the orientation of individual S_i measurements (Fig. 6) may be due to the following factors: (1) measurement error ±10° due to the difficulty of measuring S_i in garnets in situ (Cruden and Charlesworth, 1976), (2) normal variation ±10° in foliations inherent in all penetrative foliations due to their anastomosing pattern (Timms, 2002), (3) garnet nucleation at different times during the development of eventual S_i, (4) folding of future S_i before garnet overgrowth, (5) later rotation of garnets, or (6) later faulting. Factors 1 and 2 are inherent to any structural study and can account for an additional ±20° variation in measured orientations. Consistency of garnet shape, morphology and composition across the outcrop excludes factor 3. Factor 4 is implicated by the pattern of S_i orientations on the outcrop surface (Fig. 7) and curvature of S_i about subhorizontal axes within individual garnets (Fig. 5), which suggest that some deformation occurred after D_1, but before and during garnet growth. The interlimb angles of macroscale S_i folds on the horizontal surface and S_i microfolds within individual garnets can account for the observed variations of 50° from the mean orientation of S_i strike and 45° from vertical in S_i dip, respectively. The lack of later folding of the external schistosity (S_2) and non-systematic distribution of S_i orientations with respect to D_2 structures excludes factor 5. Factor 6 is excluded by the consistency of all structural orientations across late brittle faults in the outcrop.

The negligible difference (2°) between the mean orientation of garnet S_i (Fig. 6) and S_1 in the Posio region (Fig. 1b) suggests that garnet S_i may be correlated with S_1 in the Posio region. Together with the above observations concerning the timing and spatial disassociation of S_i patterns with D_2 structures, it can be concluded that the orientation of garnet S_i remained unchanged during most of the development of D_2 folds and shear zones. This

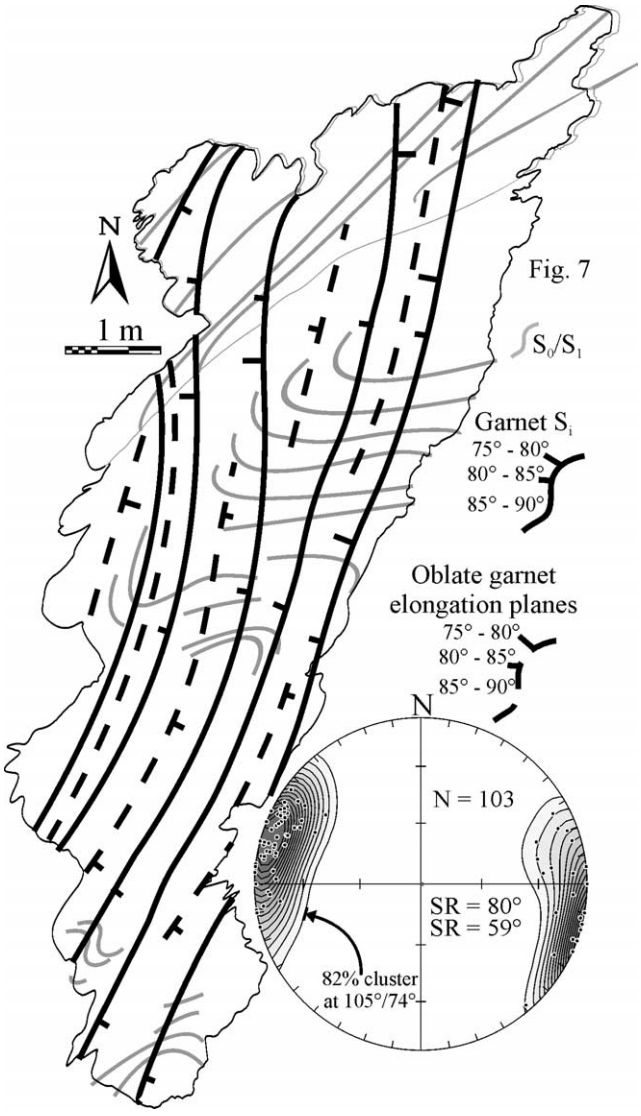

Fig. 7. Garnet S_i trajectories (drawn from 741 spatially averaged measurements) show a gentle warping not associated with F_2 folding depicted in Fig. 3. Trajectories of elongation planes of oblate garnets show a similar pattern. These are also consistently oriented as shown in the equal-area projection.

maintenance of S_i orientation during deformation is normally attributed to non-rotation of porphyroblasts due to pure shear folding (Ramsay, 1962) and/or progressive bulk inhomogeneous shortening in which fold limbs and foliations rotate around stationary porphyroblasts (Bell, 1985, 1986). However, two hypotheses incorporating rotation could explain consistent S_i orientations across later folds. The first involves the rotation of porphyroblasts until they reach a stable position with a common orientation. Mancktelow et al. (2002) and ten Grotenhuis et al. (2002) predicted this behaviour for elongate rigid particles with axial ratios >3 in simple shear. The models of ten Grotenhuis et al. (2002) allowed for strain localization in the matrix. Mancktelow et al.'s (2002) models involved varying degrees of coupling between the porphyroblast and the matrix. Although decoupling between porphyroblast and matrix encouraged stabilisation of particles with larger axial ratios, it had no effect on particles with axial ratios <3. However, garnets from the Posio outcrop are mostly spherical, and oblate garnet axial ratios are <3. Furthermore, the orientation of inclusion trails in oblate garnets is statistically indistinguishable from those of spherical garnets indicating they behaved in a similar fashion. Finally, orientations of oblate garnet elongation planes are always at a high angle (28–89°; mean at 57°) to S_e: much higher than the 5° predicted by Mancktelow et al. (2002). The second hypothesis involves a special case of flexural flow folding (Fig. 8) where porphyroblasts rotate in equal amounts and opposite direction to fold limbs effectively cancelling out their rotation with respect to fold axial planes (Williams and Jiang, 1999). This hypothesis is tested in the next section.

5. Implications for the formation of F_2 folds and shear zones

Mechanisms for folding have been traditionally divided into four kinematic end-member models (e.g. Ramsay and Huber, 1987, pp. 445–461): tangential longitudinal strain (TLS), slip folding (SF), flexural flow (FF), and homogenous pure shear (PS). Note that homogenous pure shear can only amplify pre-existing folds, and flexural slip folding is a type of flexural flow folding. Deformation partitioning (Bell, 1981, 1985) may be an integral part of some of the kinematic fold models and allows for two more end-members: progressive bulk inhomogeneous shortening (i.e. partitioned pure shear, or PPS) and partitioned flexural flow (PFF) (Fig. 8). Different mechanisms may be active solely or in combination at different times and in different places or layers throughout the history of folding. Folding mechanisms in natural rocks have been traditionally deduced from the geometry of folds and accompanying structures, such as boudins, quartz veins, slickensides, etc., and more recently by matrix–porphyroblast-fold relationships (Kraus and Williams, 1998; Stallard and Hickey, 2001). The evidence for each fold mechanism from both the outcrop and matrix–porphyroblast-fold relationships is considered in the following sections. The last section briefly compares theoretical predictions for the behaviour of porphyroblasts in shear zones with observations from the shear zones in the Posio outcrop.

5.1. Evidence from the outcrop

TLS is a special case of folding where deformation is concentrated in the fold hinge area. It requires relatively high competency contrasts between the folding layer and its surroundings (Hudleston et al., 1996) and generally produces Class 1B folds. The F_2 folds of the Posio outcrop meet none of these criteria. Competency contrast between layers is low based on the compositional and textural

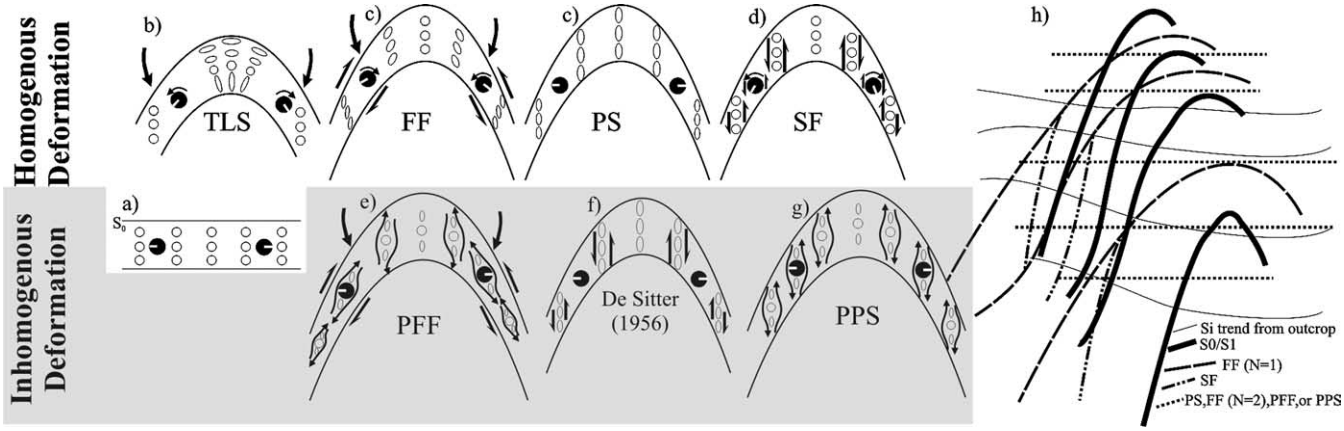

Fig. 8. Fold mechanism end members for both homogenous and inhomogeneous (deformation partitioning) layer-parallel shortening (modified from Stallard and Hickey (2001)). (a) Pre-deformed state with strain markers (empty circles) and porphyroblasts (filled circles) with an internal marker (white line). Fold axial planes are vertical for all diagrams. All models assume plane strain (i.e. no strain in the third dimension). (b) In tangential longitudinal strain (TLS), deformation is concentrated in the hinge area as the limbs rotate around it but remain undeformed internally. Porphyroblasts (along with the fold limbs) rotate with respect to the axial plane but not with respect to S_0. (c) In flexural flow (FF), fold limb rotation is accommodated by layer-parallel simple shear in the opposite direction of limb rotation. Porphyroblasts rotate with respect to both S_0 and the axial plane due to the layer parallel shear. (c) In pure shear (PS) folding, homogenous coaxial shortening results in no rotation of porphyroblasts. (d) Slip along fold axial planes produces slip folds (SF). Porphyroblasts coupled to the slipping matrix can rotate infinitely. (e) As fold limbs rotate in partitioned flexural flow, strain is partitioned into zones of simple shear parallel to S_0 surrounding areas of little to no strain. Porphyroblasts in the low strain zones do not rotate with respect to the axial plane. (f) De Sitter (1956) proposed a mechanism combining aspects of pure shear and slip folds in which coaxial deformation occurs between axial slip planes. If porphyroblasts are decoupled from the matrix, they will not rotate. (g) During progressive bulk, inhomogeneous shortening strain is partitioned into zones of simple shear parallel to the axial plane surrounding areas of little to no strain. Porphyroblasts in the low strain areas do not rotate with respect to S_0 and the axial plane. (h) Inclusion trail patterns predicted for the fold mechanisms described above superimposed on the large fold from domain III in the outcrop. The garnet inclusion trail pattern from this fold (rotated into parallelism with the horizontal reference frame) most closely matches the predictions from PS, FF ($N=2$), PFF or PPS. Patterns for fold mechanism end-members were derived from the base graphs in Fig. 9.

similarities in the matrix across domains II–VII, a lack of S_2 refraction across layering, and discontinuity of S_0/S_1 layering. Strain is concentrated in fold limbs, and the folds have an overall Class 2 geometry (Fig. 8). Unfortunately the last two observations do not help to distinguish between the remaining fold mechanisms. However, SF folds form at low mean competence and high to low competency contrast, whereas FF folds form at higher mean competence and high to low competency contrast (Donath and Parker, 1964; Twiss and Moores, 1992, p. 245). The combination of low mean competence and competency contrast expected in schists favours F_2 fold formation by SF over FF at the Posio outcrop. Discontinuity of S_0/S_1 layering may also be a result of slip along indiscrete surfaces sub-parallel to F_2 axial planes and shear zones. Problems with the inability of SF to accommodate shortening perpendicular to the axial plane can be resolved with a slight modification of the model by allowing flattening in domains between the slip planes (De Sitter, 1956, pp. 214–217) or a slight deviation of the slip plane orientation from the fold axial plane (Davis, 1995). Regardless of the modifications, SF requires evidence of significant simple shear. Likewise, FF requires similar proof. The occasional presence of synthetic, asymmetric parasitic folds is the only observation supporting a component of simple shear in the folds. On the other hand, the wealth of evidence for pure shear over the entire outcrop also applies to individual folds: in particular the symmetric, oblate shape of garnet strain shadows and presence of symmetrically buckled quartz veins and biotite grains oriented perpendicular to F_2 axial planes. Evidence for the influence of deformation partitioning is lacking in the matrix as there are no obvious crenulations and the axial planar foliation (S_2) is penetrative and closely spaced. However, the interpretation of garnet S_i (discussed below) can be easily accommodated by both the PPS and PFF models (Fig. 8). In conclusion, observations from the outcrop best support a PS, PPS or PFF fold mechanism for F_2 folds. Due to lack of asymmetry in the outcrop and the low mean competency of the schists, SF and FF are, respectively, less corroborated by the evidence, but they remain viable fold mechanisms.

5.2. Evidence from porphyroblast/matrix/fold relations

Observations of consistently oriented porphyroblast inclusion trails across folds have been often used for evidence of non-rotational porphyroblast behaviour (e.g. Fyson, 1980; Steinhardt, 1989; Forde and Bell, 1993; Aerden, 1995; Ilg and Karlstrom, 2000). Alternatively, the models of Williams and Jiang (1999) and Jiang (2001) predict these patterns in scenarios where porphyroblasts rotate from a combination of spin-induced vorticity from rotating fold limbs and layer-parallel shear-induced vorticity imparted on the porphyroblast by the matrix. Depending on the folding mechanism, these rotations can work in tandem to produce tightly folded S_i patterns or against each

other to produce a range of more open S_i folds that approach layers of no curvature (Fig. 8). The amount of curvature is inversely proportional to the parameter N (ratio of layer-parallel shear strain rate within a layer to the bulk shear strain rate) within each fold mechanism end-member. The parameter N is directly related to the competency contrast between layers. PS folding represents a special case in which porphyroblasts do not rotate relative to fold axial planes and their inclusion trail patterns remain straight (Ramsay, 1962; Williams and Jiang, 1999).

The models of Williams and Jiang (1999) and Jiang (2001) are not without restrictions. The models describe *spherical* porphyroblast behaviour in 2D for folds *outside* of shear zones. Although some garnets in the Posio outcrop are angular and oblate, and the outcrop lies within a regional shear zone, most garnets are spherical, and the outcrop has experienced relatively little non-coaxial deformation. One requirement of their models is that the folds must form due to shortening parallel to original bedding. This is often not the case when the layering being folded is tectonic and may be oblique to the shortening direction, as was likely the case for S_0/S_1 compositional layering during D_2 in the Posio outcrop. To overcome this limitation, the difference between the mean orientation of S_i measurements from each domain and limb dip reference plane for each fold was subtracted from each S_i measurement within that fold. This bulk rotation was also applied to the outcrop S_i pattern depicted in Fig. 8h. Note that this correction was applied only to conform to the Williams and Jiang (1999) method; it does not change the fact that garnet S_i patterns are not symmetrical about F_2 axial planes.

Another assumption of the models by Williams and Jiang (1999) is that porphyroblasts are perfectly coupled to their matrix. This assumption appears suspect considering the importance placed in their models on decoupling between individual layers of significantly lower competency contrast needed to produce layer-parallel shear-induced vorticity. Future models of porphyroblast behaviour during folding should account for varying degrees of coupling within the matrix and between the matrix and porphyroblast in the manners proposed by Johnson (1990b) and recently addressed by analogue models of rigid objects in shear zones (ten Grotenhuis et al., 2002; Mancktelow et al., 2002). As the models of Williams and Jiang (1999) are based on equations from fluid mechanics, they do not account for the effects of deformation partitioning oblique to layers and on scales smaller than a single layer, and therefore, cannot be used to recognize PPS and PFF as viable fold mechanisms in any study. However, a FF result from their analysis would favour PFF as an equally valid fold mechanism as would PS for PPS.

The Williams and Jiang (1999) method also requires an ideal situation where the original orientation of S_0 before folding is known and key values of limb dip from a reference plane tangential to the fold hinge (Φ), amount (angle between S_i and S_0) and sense of rotation of S_i relative to S_0 (Ω_0^G), and amount (angle between S_i and S_e) and sense of rotation of S_i relative to the fold's axial plane (Ω_1^G) can be measured. Even with these limitations, the Williams and Jiang (1999) method has so far proved useful when applied to natural folds (Stallard and Hickey, 2001). A number of assumptions were necessary to overcome the disparities between the data obtainable from this natural example and that required for the Williams and Jiang (1999) method (see Appendix A). Despite the Posio outcrop's departure from the ideal, an attempt is made to apply their method and compare data from the outcrop to their theoretical results.

Data from the limbs of each F_2 fold plotted on Ω_0^G/Φ and Ω_1^G/Φ graphs (Fig. 9) show considerable spread due to the imposed (microscale curvature and macroscale warping) and natural variations in S_i orientations described in previous sections. The degree of estimation inherent in the rotational correction of S_i data to conform to the method of Williams and Jiang (1999) resulted in ordinate intercepts displaced from zero. Regardless of these shortcomings, trends in the data are apparent. Both Ω_0^G/Φ and Ω_1^G/Φ plots restrict viable homogenous fold mechanisms to FF and PS for all folds. On Ω_0^G/Φ plots, most data points lie between the $N=1$ and $N=2$ lines for FF and $N=0.5$ and $N=1$ lines for PS. Slopes of best-fit trendlines range from 0.39 to 0.88 and are also consistent with FF, $N=1$–2, and PS, $N=0.5$–1. Their average slope is 0.61, which approximates FF $N=1$ and PS $N=0.5$. Ω_1^G/Φ plots imply slightly different constraints. Data points fall between PS $N=1$ and $N=2$ lines. As expected, based on the consistent orientation of S_i across folds, best-fit trendlines are horizontal indicating PS, $N=1$ or FF, $N=2$. Constraints for the data common to both Ω_0^G/Φ and Ω_1^G/Φ plots for all fold limbs are PS $N=1$ and FF $N=2$. These fold mechanisms and respective layer competency contrasts are what one would expect for perfectly aligned inclusion patterns crossing folds (Fig. 8h). The value of N for the schists of the Posio outcrop is estimated to be near one (i.e. no significant competency contrast between layers in the schist) because of the multiscale compositional and textural similarities in the matrix across domains II–VII, lack of S_2 refraction, and discontinuity of macroscale S_0/S_1 layering. Curiously, the data from domain I plots remarkably similar to the other fold domains even though N values should be higher in these more competent and heterogeneous turbidites. In their analysis using the method of Williams and Jiang (1999), Stallard and Hickey (2001) introduced another parameter (Z) representing the ratio of S_i rotation relative to a fold's axial plane (Ω_1^G) versus the limb dip (Φ). In the Posio outcrop, over 82% of the Z values from the fold domains fall between 0.7 and 1.3 and the mean is exactly 1.0. According to fig. 7 in Stallard and Hickey (2001) the lower limit of Z values (0.7) limits the maximum amount of FF allowed in the models to 0, 70 and 100% with assumed N values of 0.5, 1 and 2, respectively. However if $Z \approx 1$, as the mean suggests, and $N \approx 1$, as the character of the matrix suggests,

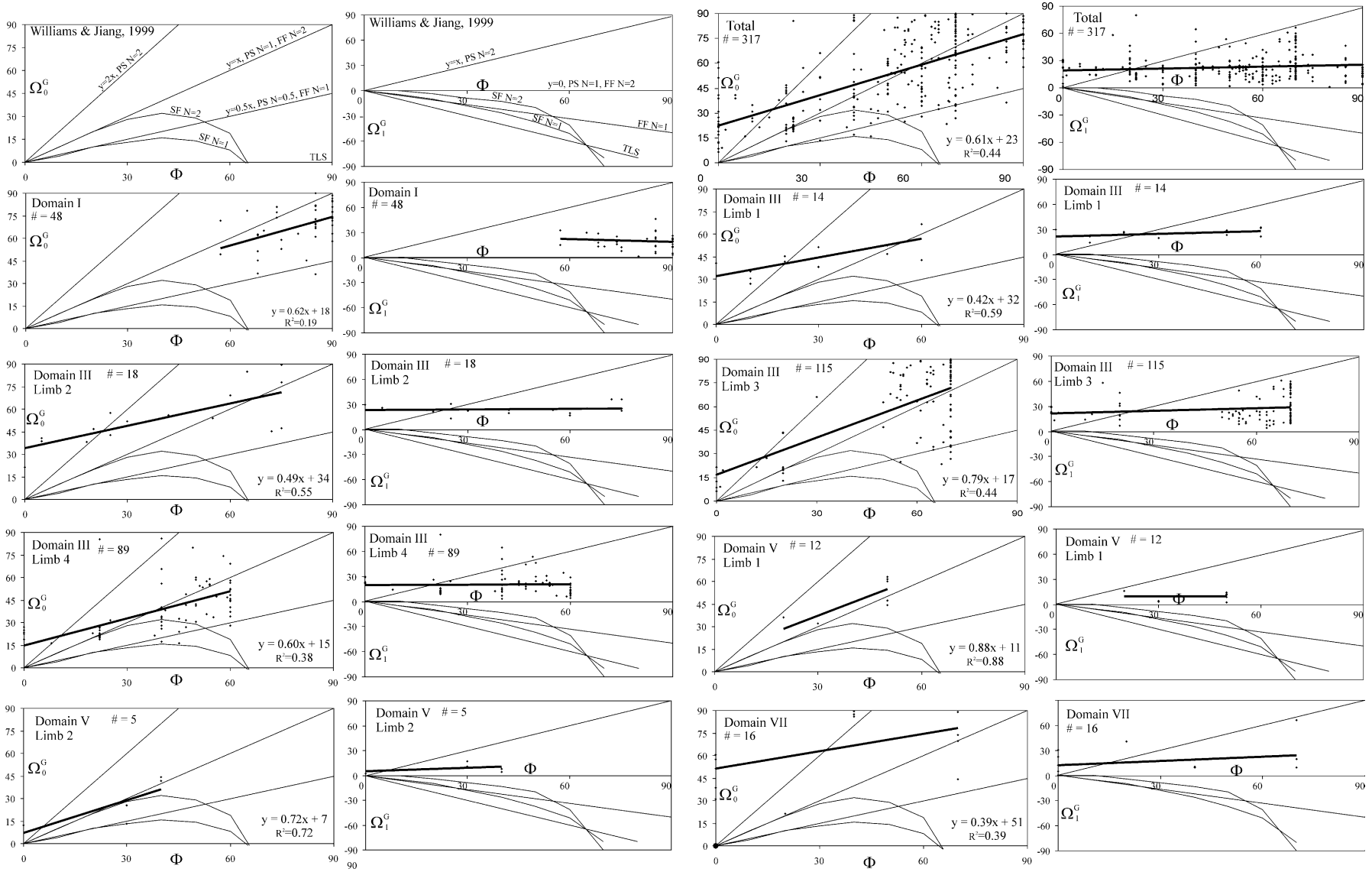

Fig. 9. Amounts of fold limb rotation (Φ) and garnet rotation relative to fold limbs (Ω_0^G) and fold axial planes (Ω_1^G) measured from each fold limb from each domain of the Posio outcrop. Φ = limb dip from a reference plane tangential to the fold hinge. Ω_0^G = angle between S_i and S_0, which represents the amount and sense of rotation of S_i relative to S_0. Ω_1^G = angle between S_i and S_e, which represents the amount and sense of rotation of S_i relative to the fold's axial plane. N = ratio of layer-parallel shear strain rate within a layer to the bulk shear strain rate. The first two graphs display $N = 1$ and $N = 2$ lines from Williams and Jiang (1999) for various fold mechanisms described in the text and in Fig. 8.

then the contribution of FF is insignificant and the dominant mechanism for the formation of F_2 folds is either PS or PPS.

5.3. Shear zones

The majority of models of porphyroblast behaviour during deformation in shear zones (Rosenfeld, 1970; Means et al., 1980; Freeman, 1985; Passchier, 1987; Masuda and Mochizuki, 1989; Gray and Busa, 1994; Samanta et al., 2002; Stallard et al., 2002) focus on non-coaxial deformation or type 2 and 3 flow (Williams and Jiang, 1999). These models predict the formation of snowball inclusion trail patterns with rotation axes parallel to the flow plane and perpendicular to the bulk flow direction in spherical porphyroblasts that have rotated more than 90° (e.g. Powell and Treagus, 1967; Schoneveld, 1977; Stallard et al., 2002). However, recent analogue models suggest porphyroblasts may not rotate due to strain localisation in the matrix (ten Grotenhuis et al., 2002) or rotate into a stable position (Mancktelow et al., 2002) if they are not perfectly coupled to the matrix. Coaxial deformation or type 1 flow is the only scenario in which porphyroblast inclusion trails remain straight or sigmoidal (Williams and Jiang, 1999). During this type of deformation, markers such as foliation rotate around the rigid porphyroblast, and one may assume that any inclusion orientation preserved inside the porphyroblast would be maintained (Ramsay, 1962; Bell, 1985, 1986). The author is unaware of any detailed studies of macroscopic porphyroblast S_i patterns in type 1 coaxial shear zones. The observation that garnet inclusion trails are only slightly sigmoidal with curvature axes perpendicular to the flow plane (Fig. 5) lends credence to the conclusion, based on outcrop observations and fold analysis, that the shear zones in the Posio outcrop formed during coaxial deformation. The remarkable consistency in orientation of garnet S_i patterns across the shear domains II, IV and VI (Fig. 6) may also be a criterion for coaxial deformation considering the large amounts of rotation inherent in non-coaxial deformation. Shear zones dominated by coaxial deformation without significant volume loss pose a problem of strain compatibility. The presence of chloritised/garnet-poor boundaries along some of the shear zones indicates that deformation within them may have involved volume loss, while their projected anastamosing geometry could accommodate large components of pure shear without compatibility problems (Hudleston, 1999). The shear zones described by Hudleston (1999) still contain a component of simple shear along the long axes of the interstitial, less-deformed pods. In the Posio outcrop, the general shape of garnet strain shadows (Fig. 5) suggests that the shear zones wrap around nearly oblate pods that are slightly extended in the vertical dimension implying that any component of simple shear during D_2 would have been subvertical, but not strong enough to form asymmetric structures.

6. Conclusions

In the Posio outcrop, composite S_0/S_1 compositional layering has been folded into a series of NE-trending F_2 folds and shear zones resulting in the development of a strong, axial planar S_2 schistosity. This schistosity wraps around garnets containing inclusion trails oriented oblique to it. Inclusion trails in the garnet porphyroblasts consistently trend N–S across the F_2 folds and shear zones. Variations in garnet S_i trends are the result of earlier macroscopic warping and microfolds geometrically unrelated to the formation of F_2 folds, shear zones, and S_2 schistosity. Structures in the outcrop and matrix indicate that D_2 folds and shear zones in the outcrop formed by NW–SE axially symmetric shortening during which garnet porphyroblasts did not rotate relative to each other, the axial plane of folding, and the shear zone boundaries. Analysis of porphyroblast/matrix/fold data by the methods outlined in Williams and Jiang (1999) indicate D_2 folds and shear zones formed by a major component of pure shear. The data is inconclusive in determining whether this was accomplished by homogenous pure shear (PS) or progressive bulk inhomogeneous shortening (PPS). On a larger scale, the PSZ is partitioned into areas dominated by coaxial or non-coaxial deformation. The Posio outcrop represents one of the domains of coaxial D_2 deformation within the PSZ.

Acknowledgements

I am grateful for Kauko Laajoki's assistance with measurements in the field. I thank Domingo Aerden, Rudolph Trouw, Paul Williams and Jurgen Kraus for their reviews of earlier versions of the manuscript, Scott Johnson and Frederick Vollmer for reviews of the current paper, Peter Hudleston for discussions on strain compatibility, Gary Solar for comments on data division and presentation, Nick Timms for fruitful discussions on all aspects of the topic, and Cees Passchier and Neil Mancktelow for pointing us in a new direction. Aaron Stallard and Dazhi Jiang were consulted to clarify parameters for the fold mechanism charts. Suggestions from Pekka Tuisku were helpful in regional correlations. Thin sections were prepared by Ulla Paakkola. Funding for this research was provided by the "Ore Processes and Geotectonics" project of the Academy of Finland (project number 34243). The Swedish Museum of Natural History is acknowledged for hosting the principal author during the final stages of manuscript preparation and for access to their SEM facilities.

Appendix A. Methods

Lack of relief in the outcrop hindered sampling and measurement of matrix fabrics. Measurement of the 3D

orientation of inclusion trails within garnet porphyroblasts was facilitated by preferential exposure of the garnets above the horizontal surface of the schists. Only garnets in which the 3D orientation of S_i was clear to two independent researchers were measured. All planar measurements are presented as dip direction and dip unless otherwise noted. The outcrop was photographed at a scale of 1:5 to produce a photomosaic of the entire outcrop. At the outcrop, all primary and secondary features appearing on Fig. 2 were traced onto the photomosaic. The location and station number of each garnet measurement was also plotted onto the photomosaic. These features were then digitised in Didger®. Coordinates for garnet measurements and digitised reference points were taken from Didger® and combined with the orientation measurements to produce lower hemisphere equal area projections (Figs. 1, 2, 4, 6 and 7) and spatially averaged maps (Figs. 1 and 7) in Spheristat©. Orientation measurements in lower hemisphere equal-area projections were contoured with Gaussian $E=3\Sigma$ counting and cluster percentages derived from triangular fabric diagrams (Vollmer, 1989) in Spheristat©. Angles between S_i, S_e and S_0/S_1 were also calculated in 3D with Spheristat©. Regional orientation data (Fig. 1) was plotted in ArcView™ with specialised fonts.

Two assumptions were necessary to overcome the disparities between the data measured from the outcrop and that required for the Williams and Jiang (1999) method. Firstly, since the axis of individual garnet S_i asymmetry is normal to the axial planes of F_2 folds, and garnet strain shadows are generally symmetric, it is impossible to observe any sense of rotation of garnets relative to S_2 (i.e. the sign of Ω_1^G cannot be directly determined). Secondly, the graphs of fig. 11 in Williams and Jiang (1999) apply only to the left limb of a fold. On the right limb, the values of Ω_0^G, Ω_1^G and Φ are reversed. Plotting of all of the data (Ω_0^G, Ω_1^G and Φ) as positive overcomes both of these problems and is justified by the relative consistency of patterns between fold limbs (Fig. 9).

All structural measurements and calculations from the Posio outcrop can be found in the online version of this article at doi:10.1016/j.jsg.2004.08.003. The author encourages other researchers to use this database to test further models on the behaviour of porphyroblasts during deformation.

References

Aerden, D.G.A.M., 1995. Porphyroblast non-rotation during crustal extension in the Variscan Lys–Caillaouas Massif, Pyrenees. Journal of Structural Geology 17, 709–725.

Bell, T.H., 1981. Foliation development: the contribution, geometry and significance of progressive bulk inhomogeneous shortening. Tectonophysics 75, 273–296.

Bell, T.H., 1985. Deformation partitioning and porphyroblast rotation in metamorphic rocks: a radical reinterpretation. Journal of Metamorphic Geology 3, 109–118.

Bell, T.H., 1986. Foliation development and refraction in metamorphic rocks: reactivation of earlier foliations and decrenulation due to shifting patterns of deformation partitioning. Journal of Metamorphic Petrology 4, 421–444.

Bell, T.H., Johnson, S.E., Davis, B., Forde, A., Hayward, N., Witkins, C., 1992. Porphyroblast inclusion-trail orientation data; eppure non son girate! Journal of Metamorphic Geology 10, 295–307.

Cruden, D.M., Charlesworth, H.A.K., 1976. Errors in strike and dip measurements. Geological Society of America Bulletin 87, 977–980.

Davis, B.K., 1995. Regional-scale foliation reactivation and re-use during formation of a macroscopic fold in the Robertson River Metamorphics, North Queensland, Australia. Tectonophysics 242, 293–311.

De Sitter, L.U., 1956. Structural Geology. McGraw-Hill, New York.

Donath, F.A., Parker, R.B., 1964. Folds and folding. Geological Society of America Bulletin 75, 45–62.

Evins, P.M., Laajoki, K., 2002. Early Proterozoic nappe formation; an example from Sodankyla, Finland, northern Baltic Shield. Geological Magazine 139, 73–87.

Evins, P.M., Mansfeld, J., Laajoki, K., 2002. Geology and geochronology of the Suomujarvi Complex; a new Archaean gneiss region in the NE Baltic Shield, Finland. Precambrian Research 116, 285–306.

Forde, A., Bell, T.H., 1993. The rotation of garnet porphyroblasts around a single fold, Lukmanier Pass, Central Alps: discussion. Journal of Structural Geology 15, 1365–1368.

Freeman, B., 1985. The motion of rigid ellipsoidal particles in slow flows. Tectonophysics 113, 163–183.

Fyson, W.K., 1980. Fold fabrics and emplacement of an Archean granitoid pluton, Cleft Lake, Norhtwest Territories. Canadian Journal of Earth Sciences 17, 325–332.

Gray, N.H., Busa, M.D., 1994. The three-dimensional geometry of simulated porphyroblast inclusion trails; inert-marker, viscous-flow models. Journal of Metamorphic Geology 12, 575–587.

Hobbs, B.E., Means, W.D., Williams, P.F., 1976. An Outline of Structural Geology. John Wiley and Sons, New York.

Hudleston, P., 1999. Strain compatibility and shear zones: is there a problem? Journal of Structural Geology 21, 923–932.

Hudleston, P.J., Treagus, S.H., Lan, L., 1996. Flexural flow folding; does it occur in nature? Geology 24, 203–206.

Ilg, B.R., Karlstrom, K.E., 2000. Porphyroblast inclusion trail geometries in the Grand Canyon; evidence for non-rotation and rotation? Journal of Structural Geology 22, 231–243.

Jeffery, G.B., 1922. The motion of ellipsoidal particles immersed in a viscous fluid. Proceedings of the Royal Society of London A102, 161–179.

Jiang, D., 2001. Reading history of folding from porphyroblasts. Journal of Structural Geology 23, 1327–1335.

Johnson, S.E., 1990a. Deformation history of the Otago schists, New Zealand, from progressively developed porphyroblast–matrix microstructures: uplift-collapse orogenesis and its implications. Journal of Structural Geology 12, 727–746.

Johnson, S.E., 1990b. Lack of porphyroblast rotation in the Otago schists, New Zealand: implications for crenulation cleavage development, folding and deformation partitioning. Journal of Metamorphic Geology 8, 13–30.

Johnson, S.E., 1993. Testing models for the development of spiral-shaped inclusion trails in garnet porphyroblasts: to rotate or not to rotate, that is the question. Journal of Metamorphic Geology 11, 635–659.

Johnson, S.E., 1999. Porphyroblast microstructures; a review of current and future trends. American Mineralogist 84, 1711–1726.

Kärki, A., Laajoki, K., Luukas, J., 1993. Major Paleoproterozoic shear zones of the central Fennoscandian Shield. Precambrian Research 64, 207–233.

Kraus, J., Williams, P.F., 1998. Relationships between foliation

development, porphyroblast growth and large-scale folding in a metaturbidite suite, Snow Lake, Canada. Journal of Structural Geology 20, 61–77.

Kraus, J., Williams, P.F., 2001. A new spin on "non-rotating" porphyroblasts; implications of cleavage refraction and reference frames. Journal of Structural Geology 23, 963–971.

Laajoki, K., Tuisku, P., 1990. Metamorphic and structural evolution of the early Proterozoic Puolankajärvi Formation, Finland. Part I. Journal of Metamorphic Geology 8, 357–374.

Mancktelow, N.S., Arbaret, L., Pennacchioni, G., 2002. Experimental observations on the effect of interface slip on rotation and stabilisation of rigid particles in simple shear and a comparison with natural mylonites. Journal of Structural Geology 24, 567–585.

Masuda, T., Mochizuki, S., 1989. Development of snowball structure; numerical simulation of inclusion trails during synkinematic porphyroblast growth in metamorphic rocks. Tectonophysics 170, 141–150.

Means, W.D., Hobbs, B.E., Lister, G.S., Williams, P.F., 1980. Vorticity and non-coaxiality in progressive deformations. Journal of Structural Geology 2, 371–378.

Passchier, C.W., 1987. Stable positions of rigid objects in non-coaxial flow—a study in vorticity analysis. Journal of Structural Geology 9, 679–690.

Passchier, C.W., Trouw, R.A.J., Zwart, H.J., Vissers, R.L.M., 1992. Porphyroblast rotation: eppur si mouve? Journal of Metamorphic Geology 10, 283–294.

Powell, D., Treagus, J.E., 1967. On the geometry of S-shaped inclusion trails in garnet porphyroblasts. Mineralogical Magazine 36, 453–456.

Ramsay, J.G., 1962. The geometry and mechanism of formation of "similar" type folds. Journal of Geology 70, 309–327.

Ramsay, J.G., 1967. Folding and Fracturing of Rocks. McGraw-Hill, New York.

Ramsay, J.G., Huber, M.I., 1987. The Techniques of Modern Structural Geology. Volume 2: Folds and Fractures. Academic Press, London.

Ramsay, J.G., Lisle, R., 2000. The Techniques of Modern Structural Geology. Volume 3: Applications of Continuum Mechanics in Structural Geology. Academic Press, London.

Rosenfeld, J.L., 1970. Rotated Garnets in Metamorphic Rocks. Geological Society of America (GSA), Boulder, CO.

Samanta, S.K., Mandal, N., Chakraborty, C., Majumder, K., 2002. Simulation of inclusion trail patterns within rotating synkinematic porphyroblasts. Computers and Geosciences 28, 297–308.

Schoneveld, C., 1977. A study of some typical inclusion patterns in strongly paracrystalline-rotated garnets. Tectonophysics 39 (1-3), 453–471.

Stallard, A., Hickey, K., 2001. Fold mechanisms in the Canton Schist; constraints on the contribution of flexural flow. Journal of Structural Geology 23, 1865–1881.

Stallard, A., Ikei, H., Masuda, T., 2002. Numerical simulations of spiral-shaped inclusion trails; can 3D geometry distinguish between end-member models of spiral formation? Journal of Metamorphic Geology 20, 801–812.

Steinhardt, C.K., 1989. Lack of porphyroblast rotation in non-coaxially deformed schist from Petrel Cove, South Australia, and its implications. Tectonophysics 158, 127–140.

Talbot, C.J., 1970. The minimum strain ellipsoid using quartz veins. Tectonophysics 6, 47–76.

ten Grotenhuis, S.M., Passchier, C.W., Bons, P.D., 2002. The influence of strain localisation on the rotation behaviour of rigid objects in experimental shear zones. Journal of Structural Geology 24, 485–499.

Timms, N., 2002. A tectonic evolution through microstructures: Orford to Piermont area of the New England Appalachians, west-central New Hampshire, USA. PhD Thesis, James Cook University, Queensland Australia.

Tuisku, P., Laajoki, K., 1990. Metamorphic and structural evolution of the Early Proterozoic Puolankajärvi Formation, Finland. Part II. Journal of Metamorphic Geology 8, 375–391.

Twiss, R.J., Moores, E.M., 1992. Structural Geology. W.H. Freeman and Company, New York.

Vaasjoki, M., Karki, A., Laajoki, K., 2001. Timing of Palaeoproterozoic crustal shearing in the central Fennoscandian Shield according to U–Pb data from associated granitoids, Finland. Bulletin of the Geological Society of Finland 73, 87–101.

Visser, P., Mancktelow, N.S., 1992. The rotation of garnet porphyroblasts around a single fold, Lukmanier Pass, Central Alps. Journal of Structural Geology 14, 1193–1202.

Vollmer, F.W., 1989. A triangular fabric plot with applications for structural analysis. Eos 70, 463.

Williams, P.F., Jiang, D., 1999. Rotating garnets. Journal of Metamorphic Geology 17, 367–378.